

# Advanced Image Segmentation Techniques for Neural Activity Detection via C-fos Immediate Early Gene Expression

1<sup>st</sup> Peilin Cai  
Wuhan University

**Abstract**—This paper investigates the application of advanced image segmentation techniques to analyze C-fos immediate early gene expression, a crucial marker for neural activity. Due to the complexity and high variability of neural circuits, accurate segmentation of C-fos images is paramount for the development of new insights into neural function. Amidst this backdrop, this research aims to improve accuracy and minimize manual intervention in C-fos image segmentation by leveraging the capabilities of CNNs and the Unet model. We describe the development of a novel workflow for the segmentation process involving Convolutional Neural Networks (CNNs) and the Unet model, demonstrating their efficiency in various image segmentation tasks. Our workflow incorporates pre-processing steps such as cropping, image feature extraction, and clustering for the training dataset selection. We used an AutoEncoder model to extract features and implement constrained clustering to identify similarities and differences in image types. Additionally, we utilized manual and automatic labeling approaches to enhance the performance of our model. We demonstrated the effectiveness of our method in distinguishing areas with significant C-fos expression from normal tissue areas. Lastly, we implemented a modified Unet network for the detection of C-fos expressions. This research contributes to the development of more efficient and automated image segmentation methods, advancing the understanding of neural function in neuroscience research.

**Keywords**—*Medical Image Segmentation, U-Net, Segment Anything Model, C-fos*

## I. INTRODUCTION

*A. Background on C-fos immediate early gene and its importance in neuroscience research.*

The C-fos immediate early gene, an instrumental protein-coding gene, plays a pivotal role in the regulation and functioning of the nervous system. Its importance in the field of neuroscience is significant; it serves as a widely recognized marker for neural activity. The gene is notably characterized by its rapid and transient induction in response to a broad range of stimuli, which can be sensory, physiological, or pharmacological. Consequently, C-fos expression is frequently utilized as a proxy for neural activity in various domains of neuroscience research, such as learning, memory, addiction, and beyond [1].

The expression of the C-fos gene can be visually represented through a technique known as immunohistochemistry [2]. This method involves the use of

specific antibodies to recognize and bind to the C-fos protein in tissue samples, illuminating its presence. However, the analysis of the resultant C-fos images can be intricate and challenging due to the intricate nature of neural circuits and the considerable degree of variation in the gene's expression patterns.

To address these challenges, image segmentation could be employed. Image segmentation is a process that classifies the pixels in an image into different categories, enabling researchers to distinguish the C-fos objects from the background. This in turn aids in the identification and quantification of C-fos expression across distinct regions of the brain.

The precision of segmentation in C-fos images is crucial for interpreting experimental results, shaping new hypotheses, and unraveling deeper insights into neural function. Nonetheless, manual segmentation, the traditional approach, presents several limitations. It is not only time-consuming and labor-intensive, but it also subjects the results to inter-observer variability, making consistency and replicability a challenge.

In light of these difficulties, the development of automated image segmentation methods has come to the forefront of neuroscience research. A promising approach lies in the use of advanced machine learning techniques, specifically convolutional neural networks (CNNs). Unet [6], a type of CNN, has shown significant potential. Its high accuracy and efficiency in numerous image segmentation tasks make it a powerful tool for automating and enhancing the analysis of C-fos expression. This cutting-edge approach holds potential to revolutionize neuroscience research, streamlining the process and facilitating new discoveries.

The principal objective of this research is to develop, a workflow utilizing CNNs and the Unet model for automating the segmentation of C-fos images, consequently facilitating more accurate and efficient analysis of neural activity markers. At the same time, we use the current advanced Segment Anything Model [5] combined with image classification to reasonably integrate the proportion of data in the training set in order to reduce the efficiency cost of the model to learn effective information. Other sub-objectives include reducing manual segmentation effort, enhancing

consistency in results, or providing a framework for scalability in analyzing large image datasets.

## II. METHODS AND RESULT

### A. Workflow

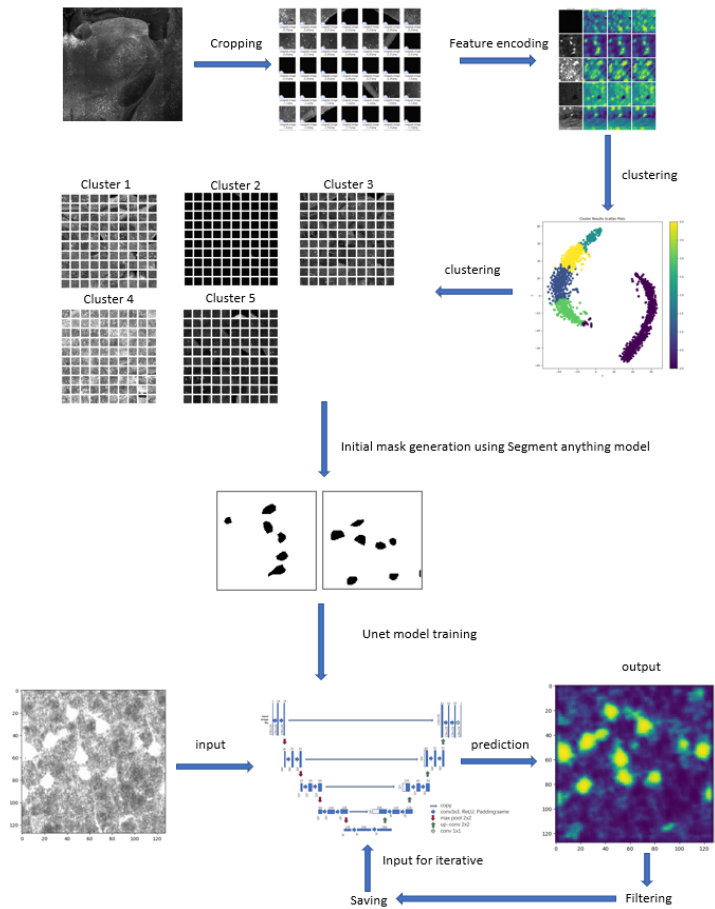


Fig. 1. Our workflow is thus composed. It can be roughly divided into five steps: crop-classify-train-predict-iterate.

In this study, we developed a pipeline for image processing for object segmentation. Briefly, we first cropped the image into small tiles. Based on features extracted, we then performed k-means clustering in generating different groups of images tiles. From each cluster, we randomly selected representative tiles to generate mask images. These data will be used as the training dataset in our Unet network for object segmentation. The predicted image would then be used in the training process. Thus, a feedback loop would be formed to further fine-tune the model.

### B. Preprocessing of C-fos immediate early gene expression image.

C-fos immediate early gene expression can be visualized using immunohistochemical techniques, using which to conduct special image sampling can allow us to obtain C-fos immediate early gene expression images with distinct marker characteristics. However, due to the uneven

structure of the mouse brain, the distribution of expressed image features also appears to be very uneven which is visible to the naked eye.

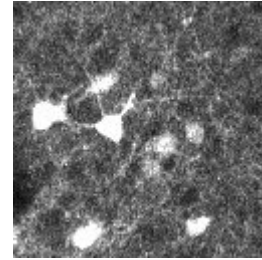


Fig. 2. A typical sample of C-fos immediate early gene expression. In this image, a background composed of sparse white highlights and black screens appears with large and obvious white blocks.

We used a special chemical labeling method to distinguish areas with significant C-fos expression from normal tissue areas. In the sample map (see Figure 1), the white patches are the expression of C-fos immediate early gene but the white highlights are not.

In the images after the 128x128 standard cropping of preprocessing, we have roughly summarized five types of samples with obvious characteristics in feature distribution.

Crop the image into different size (128x 128 pxl)

First we obtained the image to be segmented, which has a huge resolution (10231x7162), and obviously we cannot directly feed this kind of image into the network as a dataset for processing, which would not only incur huge labeling costs but also greatly reduce the segmentation speed and accuracy. Therefore, cropping the samples is a pre-processing step that we must do.

In fact, considering the size of a single segmentation task, the best size of samples suitable for processing by the Unet network is between 64x64 and 572x572, among which we consider 128x128 to be a suitable choice.

The next task is very simple: call the tool library to crop the loaded image object into several png images with a resolution of 128x128 according to the method of horizontal and then vertical orientation, and then save them locally.

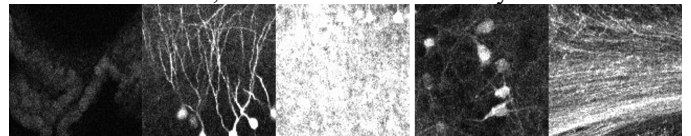


Fig. 3. Five types of samples. From left to right, the sequence is as follows: (a) The presence of active neural cells is too sparse, leaving the overall background in a black state and without significant C-fos gene expression regions; (b) There are several distinct regions of C-fos gene expression, but nerve cells have distinct white "tails" (tissues connecting nerve cells) that interfere with sample recognition; (c) Due to the dense presence of nerve cells and other reasons, C-fos genes are highly concentrated and actively expressed, making the overall background in a bright white state, making it difficult to identify independent C-fos blocks. However, the above diagram shows an extreme situation, most of the time type c is as easy to distinguish as type b and d, but the labeling workload is a bit more; (d) There are several regions with significant C-fos gene expression, which is in sharp contrast to the overall black background, and the difficulty of recognition and learning are low; (e) Although there is no obvious trace of C-fos gene expression, due to the presence of a large number of nerve fibers, the overall appearance of white stripes appears.

For these five types of samples, we adopt different labeling strategies for better performance of our model.

### Adoption of different cropping methods

We tested the usage of cropping images with a moving window. As shown below, the moving-window approach could provide a better handling of the image edges compared with the one without using moving window.

### C. Image feature extraction and clustering for training dataset selection

To automate the classification, we try to train a model that automatically extracts features and implements constrained clustering. Finally we decide to use an unsupervised learning model based on CNN(AutoEncoder) to get the feature representing vector.

Similarly, our AutoEncoder specifies a resolution of 128x128 for the input image. The structure of our designed AutoEncoder consists of three convolutional layer followed by pooling layers and three convolutional layer followed by up-sampling layers, each convolutional layer activated by a ReLU. After the images are read, we let AutoEncoder's model perform unsupervised encoding training, considering the sample size is around 1500, we set the number of iterations (epoch) to 20 and the batchsize to 32. This training is very brief, and after finishing it, we randomly let the model predict a few images to check the effect, and then we can use it for feature extraction.

The clustering will give five clusters as the result, and we can visualize the distribution of the number of each cluster by this graph.

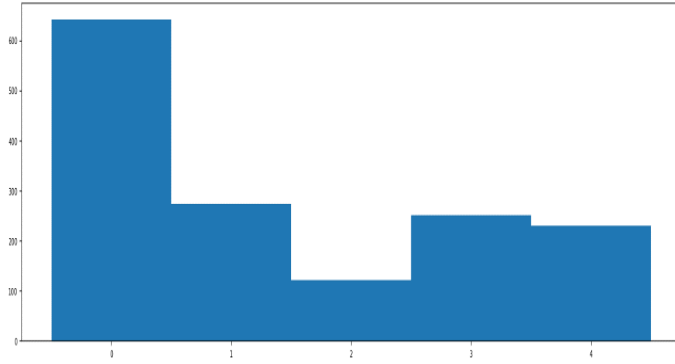


Fig. 4. The histogram reflecting the number of samples contained in each cluster.

This extremely uneven distribution warns us that if we set up the training set and the sample set according to the random sampling method, there is a consequence that the model will show a very different degree of accuracy for the samples of different clusters. And we can see that the samples of cluster0 are almost pure black images. Once the training set is obtained by random sampling, it will be filled with a large number of original images and mask files that are punitive to training, resulting in a significant dilution of the model's ability to predict truly meaningful samples.

The process of AutoEncoder learning encoding is somewhat random, so there will be small differences in the classification

results after each learning process. But in general we can see that the classification is reliable in four ways:

(1)After each clustering, the number of samples in each cluster is arranged incrementally, and the ratio is always approximately 1:2:2:2.4:5.4. For example, in one of our more satisfactory classifications (using our training model "5-6-autoencoder-model.h5"), the ratio of the sample distribution is 120:234:238:287:648.

(2)Sampling from the clustering results, and then observing the encoding results of its intermediate layers. Since the shape of the encoding result is 16x16x8, it needs to be converted to grayscale to display the image. Here the final dimensions are taken as minimum, maximum and standard deviation respectively.

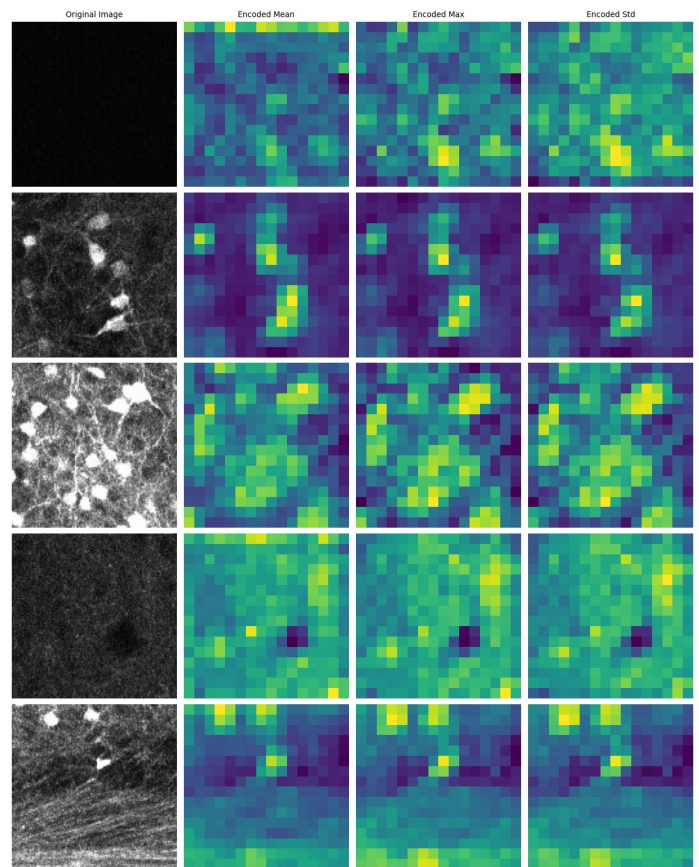


Fig. 5. Encoding Results. From top to bottom are the original images selected from the five classes of clustering results with their encoding results. It can be seen that the various types of images have significantly different feature distributions.

The encoded features are downscaled to a two-dimensional space using the t-SNE method, and then scatter plots are drawn. The t-SNE method can preserve the local structure of the data as much as possible by preserving the relative distances between data points, and then calculates the similarity between data points and constructs a probability distribution in a high-dimensional space based on the

calculated similarity. Next, it constructs another probability distribution in a low-dimensional space and tries to make the two distributions as similar as possible. To achieve this, t-SNE uses optimization methods such as stochastic gradient descent to minimize the Kullback-Leibler scatter (KL scatter).

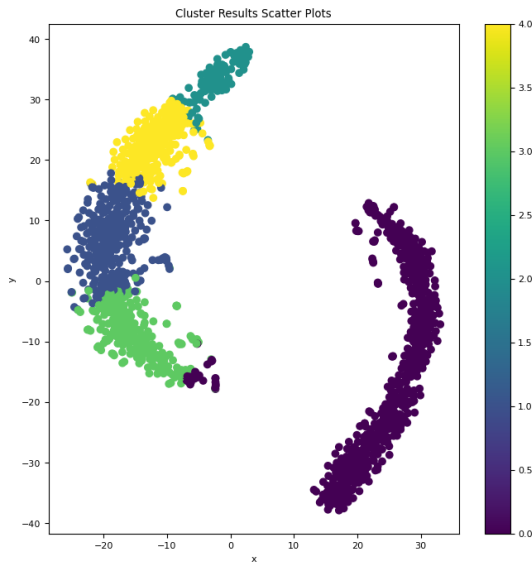


Fig. 6. **The scatter plot drawn from our results of this classification.** The encoding results in an array of 1517x8x8x16 dimensions, which becomes 1517x2 points after dimensionality reduction. We can find the corresponding points based on the index of the clusters and then draw a scatter plot.

We can directly show the images of each cluster to visualize the similarity of images within each cluster and the difference of images between clusters.

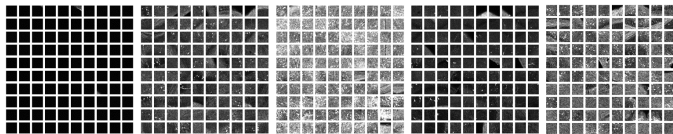


Fig. 7. **Results of a clustering with ideal performance.** From left to right, The sequence corresponds to the indexes 0-4 of the clusters, and also to the results of our previous manual classification a-e. Combined it seems that the images are classified according to the features of average brightness and texture, more in line with our initial manual classification. Each image is placed in a 10x10 grid with the contents of the corresponding cluster sampled in turn.

It can be seen that: cluster0 tells us it is a class of highly sparse, extremely dark samples with an almost all-black image array; cluster1 is a class carrying a concentrated distribution of C-fos with tail traces; cluster2 is a class with active C-fos expression; cluster3 is a slightly sparse class with a clear contrast between C-fos gene expression and background; and cluster4 is filled with patterns like lines drawn by a large number of nerve fibers.

#### D. Cropping and combination with method of overlapping region

If we take a generic crop and split approach, like this:

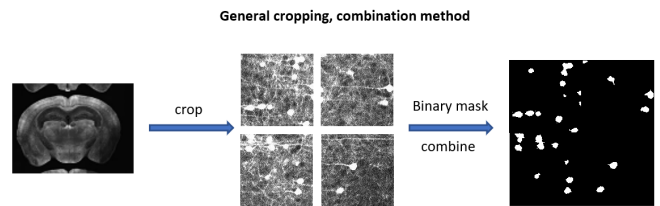


Fig. 8. **The general method**

It can be seen that the predicted results become very abrupt and discontinuous at the edges. To solve this problem, we use cropping and combination with method of overlapping region (Sliding windows cropping, combination method), like this:

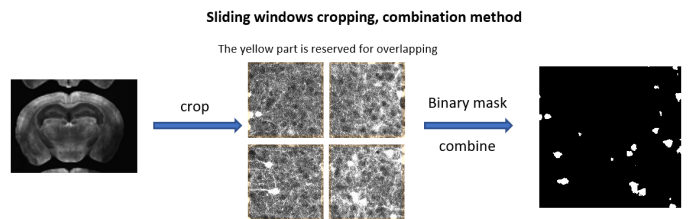


Fig. 9. **Our method**

As you can see, our cropping strategy solves the possible edge discontinuity problem above, which can be seen more clearly by this comparison chart below.

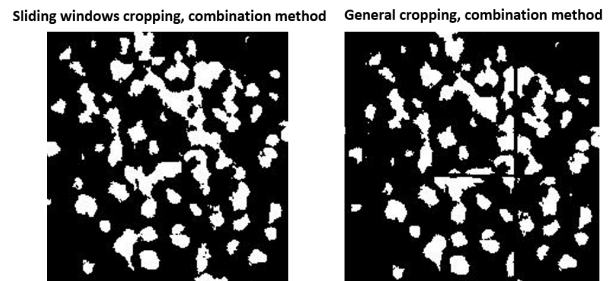


Fig. 10. **Comparison of the prediction results of the two methods**

The presence of overlapping region makes our information articulation and edge processing smooth and logical. The size and location of the overlapping regions can be adapted to specific tasks and needs. In general, larger overlapping regions can provide better information convergence and boundary processing, but increase the computational complexity. Therefore, the size and performance requirements of the overlapping regions need to be considered when designing image segmentation algorithms. The overlapping used in this project is 128x128 sample image centered outward by 4 pixels.

#### E. Image labeling using Manual and automatic approaches. Manual labeling

Here we used labelme as the labeling tool, which is accurate however time consuming.

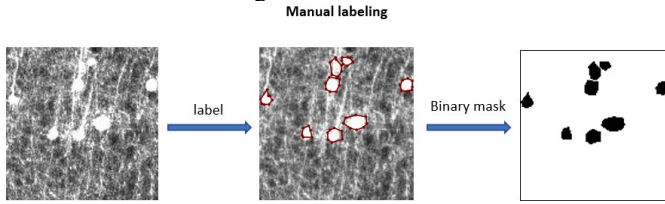


Fig. 11. Manual method

### Automatic labeling

We tested the labeling capability of the segment anything model in the mask image generation. It potentially could be a high throughput however require human input for the correction.

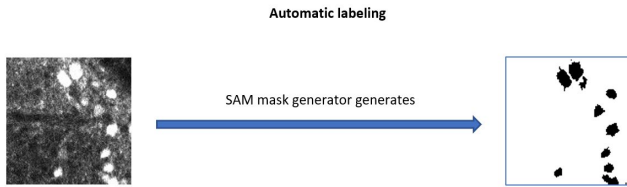


Fig. 12. Automatic method

### Semi-automatic labeling

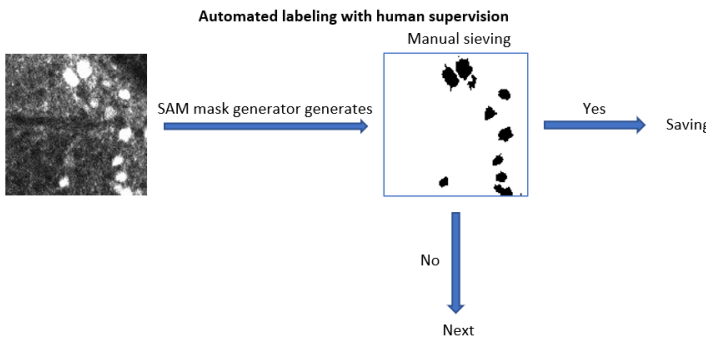


Fig. 13. Semi-automatic method

Moreover, we tested the SAM segmentation with human input. The role of human supervision here is to screen the segmentation results that pass visual observation. Excluding the possibility of an overall pixel shift in the image to be reviewed, the human reviewer's naked-eye judgment results are actually very realistic.

This semi-automatic supervised process can be introduced during training set generation or during prediction on the test set. The former helps us to generate more accurate samples, while the latter helps us to correct the capability of the current model and generate a new training set for iterative training. In this project, we introduced only the latter considering the overly large number of cropped samples.

### F. The concept and structure of Unet and its application in biomedical image analysis.

Unet network is an improved fully convolutional network, of which the original intention is to be used in medical image

segmentation. It can work with very few training images and yields more precise segmentations. The main idea in the Unet network is to supplement a usual contracting network by successive layers, where pooling operators are replaced by upsampling operators. Hence, these layers increase the resolution of the output.

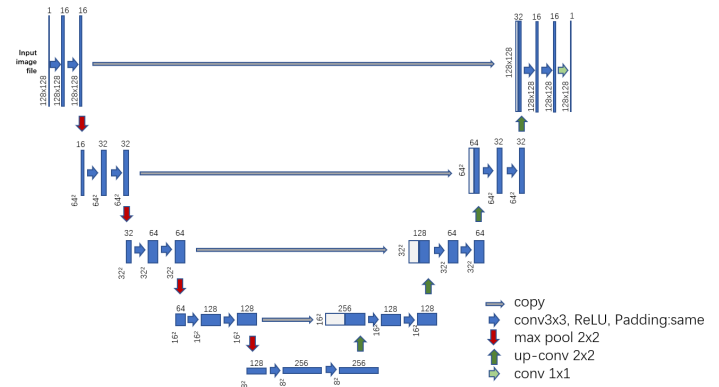


Fig. 14. U-net architecture (example for  $8^2$  pixels in the lowest resolution). Each blue box corresponds to a multi-channel feature map. The number of channels is denoted on top of the box. The x-y-size is provided at the lower left edge of the box. White boxes represent copied feature maps. The arrows denote the different operations.

The network architecture is illustrated in Figure 3. It consists of a contracting path (left side) and an expansive path (right side) as what it is in an original Unet.

The contracting path consists of recycled convolution layers and pooling layers. In order to make the output consistent with the size of the input image, we carefully removed the cropping portion, and set the padding parameter to "same" during convolution. Each convolution core has a size of  $3 \times 3$ , and the convolution result is rectified by ReLU. In the contracting path, after two convolutions in a layer are completed, the pooling layer is responsible for performing down sampling, doubling the number of feature channels. Expansive path performs the same convolution, but ultimately reduces the number of characteristic channels by half through  $2 \times 2$  up-convolution. At the same time, there will be a concatenation with the correspondingly collapsed feature map from the contracting path. At the final layer a  $1 \times 1$  convolution is used to map each 16 component feature vector to the desired number of classes.

In this paper, we use Unet network to train several models that can automatically realize Cfos detection. We have almost followed the original structure of the Unet network, only adjusting some of its parameters (see Figure 3) : the resolution of the input image has been fixed at  $128 \times 128$ , because a smaller resolution is conducive to improving the reading rate of each image. The resolution of the original pattern itself is already extremely large, and dividing it into  $128 \times 128 \times 4N$  is more suitable for extracting effective information than dividing it into  $256 \times 256 \times N$  samples. The padding parameter is set to "same", which is to make the input image consistent with the output image size. At the same time, we omit the steps of cropping in the network.

TABLE I. SCORES CORRESPONDING TO DIFFERENT TRAINING METHODS

Method	MIoU score	F1 score
Untrain	0.0122	0.0234
Simply Train ①	0.6917	0.7952
Cluster Train ②	0.7312	0.8264
SAM Train ③	0.6045	0.6823
SCT ④	0.6731	0.7292
SCIT ⑤	0.6837	0.7367

This table lists the MIoU scores of different methods with F1 scores. It can be seen that the model works very poorly in the untrained case. Therefore the usefulness of training our model can be reflected by the scores.

①: It is a simple training by manually labeled dataset with samples randomly sampled from the cropping results, resulting in the vast majority of the dataset being almost pure black images.

②: It is a dataset artificially sampled after classification using AutoEncoder. I reduced the number of samples of black images and increased the number of samples of the more dense Cfos images, and the results are better than ①. It is worth noting that both our training set (156) and validation set (34) are smaller in size than the SAM method due to the high cost of manual labeling.

③: The dataset is from SAM automatic model. Characteristically, the dataset size is greatly increased, and the training set is extended to 245 and the validation set is extended to 180. This part of the dataset is sampled by random selection.

④: SAM Cluster Train, where the data set after conscious classification is used for training.

⑤: SAM Cluster Iteration Training, where the model's predictions on the test set are submitted to human supervision and, if reasonable, saved as a new dataset for iterative training. Combining the above information we can judge that the accuracy of the manually labeled dataset is higher, but the time cost consumed is also higher. The model with SAM roughly makes up for this loss in time cost savings, despite the decrease in accuracy. Finally, the human intervention supervised iterative approach improves the accuracy of the SAM model segmentation again with less labor cost and is adopted as our final solution.

In addition to this, the effect of sample size on our scores in the case of our fixed test set is as follows: (epoch = 15)

TABLE II. SCORES CORRESPONDING TO DIFFERENT SAMPLE SIZES

Training set size	MIoU score	F1 score
0	0.0122	0.0234
5	0.4415	0.4922
30	0.5904	0.6367
80	0.6521	0.6980
150	0.6731	0.7292
250	0.6237	0.6611

It can be seen that a serious overfitting phenomenon occurs when the sample training set size reaches 250. And until the sample size reaches 80, the model is in an under-trained state.

### G. Apply to high resolution images

Our final segmentation result is shown in the following figure:

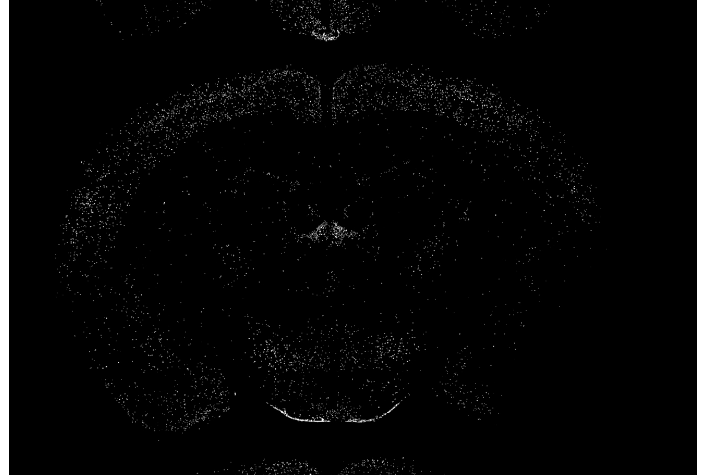


Fig. 15. **Final Work** This result is obtained by the model predicting all the cut images one by one and then recomposing the predicted results into a complete image.

## III. DISCUSSION

C-fos per se is an early immediate gene that partially reflect the functional activity of neuronal populations. C-fos expression would increase when the calcium dynamics was changed due to activity change. Thus, the neuroscience field has adopted this approach to identify the associated brain structures to be involved in a specific function/context. The throughput of generating these images increases. Manual detection or quantification of these images would consume time and effort. Machine learning based image detection or segmentation approaches has been developed.

The method of training models in AutoEncoder determines the fact that each newly trained model does not generate exactly the same classification results for the samples to be pre-processed that we give.

However, the features of our samples themselves and the way the convolutional features are extracted also dictate that each fully trained new model will not generate classification results that differ too much from each other.

Our research provides insights into the value of automated image segmentation techniques in neuroscience, specifically in the analysis of C-fos immediate early gene expression. By utilizing Convolutional Neural Networks (CNNs) and the Unet model, we have effectively demonstrated the potential of these techniques in handling complex image segmentation tasks in a high-throughput, consistent, and accurate manner.

A significant advancement in our study is the development of a workflow that incorporates various pre-processing steps like cropping, feature extraction, and clustering for the training dataset selection. The adoption of these pre-processing strategies has shown promising results in simplifying the complexity of the C-fos images while retaining the essential attributes that signify neural activity.

Our study also employed an AutoEncoder model for feature extraction, which facilitated effective clustering of the

images based on their distinct characteristics. This unsupervised learning approach minimizes bias and allows for more objective categorization of the images. However, it is worth noting that while this process was generally successful, certain classifications showed some randomness, which could be addressed in future research to optimize the precision of our model.

The manual and automatic labeling approaches used in this study have also demonstrated significant potential for efficiency in handling large-scale datasets. Although the manual method was time-consuming, it provided an accurate benchmark for validating the performance of the automatic labeling technique. Our findings highlight the need for a balance between automation and human supervision to ensure both the accuracy and efficiency of the model.

Furthermore, the modified Unet network model we implemented displayed remarkable capability in distinguishing regions of significant C-fos expression from normal tissue areas. The customized design and parameters of our model made it adaptable to the specific characteristics of our dataset, enhancing its performance.

Nevertheless, there are several avenues for improvement and future research. The results demonstrated variations in accuracy between different clusters, suggesting the need for more sophisticated training set-up procedures to mitigate such inconsistencies. Additionally, although our model was effective for the C-fos images used in our study, it remains to be seen how it would perform with other types of biomedical images. Further studies could explore its versatility and adaptability to different types of datasets and contexts.

In conclusion, our study has shown that automated image segmentation techniques, particularly the application of CNNs and the Unet model, can play a vital role in advancing neuroscience research. They not only streamline the analysis of complex neural images but also open avenues for gaining deeper insights into neural function and activity. By continuing to refine these techniques, we can significantly advance our understanding of the nervous system, leading to potential breakthroughs in various areas of neuroscience, such as memory, learning, and addiction research.

## IV. ENVIRONMENT AND PROCESSES DETAILS

### A. System environment.

Sam Generator:  
(Google Colab)  
Python version = 3.10  
Pytorch version = 2.0.1  
Cuda version = 11.8

Unet Model Training and Prediction  
Python version = 3.9.16  
TensorFlow version = 2.10.0  
Numpy version = 1.24.3  
GPU/CPU = GTX1650  
Labelme (python = 3.7)

### B. Image preprocessing

#### 1) Image cropping:

The Unet model does not perform as well in predicting locations near the edges as it does in the centre of the image. This is due to many reasons, such as the fact that the manually labelled mask in the training set does not cover the edges well. The authors of Unet designed Unet using skip connections to make optimisations, but did not completely solve the problem that exists at the edges of images. In our approach, we try to transform image edges into image centres, crop and splice with a sliding window so that the centre prediction covers all edge positions, to achieve a more accurate application of Unet on high resolution images, with the following strategy:

Crop: After reading a high-resolution image of HxW, the image is padded outwards with (a) pixel size of solid black, so that the image size changes to  $(H+2a) \times (W+2a)$ . Based on this image, a window of size  $X^2$  is created at point (0,0) to store the image inside this window, and the content of the image is the content inside the rectangle from (0,0) to (X,X) based on the new image. Then move the window to the right by  $(X-2a)$  pixels and see if the image can be captured inside the rectangle of size  $X^2$ , if so, save the image inside the rectangle and then move it further to the right using this method; if not, set the horizontal coordinate of the upper left corner of the window to 0 and increase the vertical coordinate by  $(X-2a)$  pixels, save the image and then move it to the right again. Eventually we will get many cropping results with an overlapping area of  $2a \cdot X$  size for any adjacent window images at the top and bottom. The cropping results are numbered according to the number of right and bottom shifts, e.g. the image in the first row of windows with 3 right shifts is named 0-2.jpg.

Combination: The way to combine (processed) crop results is to further crop all the images, crop off the edges of the original crop result of size  $X^2$  with length a to get the center image of size  $(X-2a)^2$ , and then combine all crop centre images in the order mentioned.

For our Unet model, we set X to 128 and a to 4 to match the size of the input image.

The HxW high-resolution image size of mouse brain slices used in our experiments was 10231x7162, and 85x59 images were segmented.

By this method, we circumvent the pitfalls of edge segmentation very effectively.

#### 2) mask image generation:

##### Manual labeling using labelme

labelme is an open source graphical image annotation tool written in Python and using Qt for its graphical interface. It is a software with a simple and interactive interface. It can be used to annotate our images by launching it from the command line in a specific environment. The annotation is also simple: create a new polygon, fill in the corresponding label name and then draw a polygon around the part of the image we want to label with features. We can then batch generate json files with our annotation information, and these

files can be used by another simple Python program to generate mask images corresponding to the cropped image samples in our training set.

This gives us a pair of samples, the images and the labels of the images. They can be fed into our network as a set of samples, and the network will optimise the parameters of its own training process according to the labels of the training set, and finally also compare its own prediction results with the labels of the test set to evaluate its current accuracy.

#### *Automatic labeling using Segment anything model*

Segment Anything Model(SAM) is a new AI model from Meta AI that can "cut out" almost all objects in all scene. [5] We have ported the open source trial of the SAM model from github to our model. By loading the pre-trained model and calling specific methods, SAM's mask\_generator can transform an image into dictionaries that returns the contents of:

- segmentation : the mask
- area : the area of the mask in pixels
- bbox : the boundary box of the mask in XYWH format
- predicted\_iou : the model's own prediction for the quality of the mask
- point\_coords : the sampled input point that generated this mask
- stability\_score : an additional measure of mask quality
- crop\_box : the crop of the image used to generate this mask in XYWH format

The segmentation is exactly the segmentation on the basis of the original image, we can filter by the area or stability\_score to remove the segmentation that does not meet the requirements. For example, segmentation of which area is too large or too small or score is too poor. Then the remaining segmentations are merged, and the result of this merge is the mask image we need.

#### *C. Training and prediction*

The training process is simple and generic, requiring only a pre-specified dataset, followed by the TensorFlow generic training model approach. During training, epoch and batchsize can be specified according to the sample requirements.

Similarly, the prediction results are stored in some list of predictions from the test set using the TensorFlow generic model prediction approach. They can be saved as needed.

#### *D. Code availability statement*

The python scripts in Jupyter notebook format are provided as supplementary materials.<sup>1</sup>

## V. REFERENCES

- [1] Brunk, Clifford F., Kenneth C. Jones, and Thomas W. James. 1979. "Assay for Nanogram Quantities of DNA in Cellular Homogenates." *Analytical Biochemistry* 92 (2): 497–500. [https://doi.org/10.1016/0003-2697\(79\)90690-0](https://doi.org/10.1016/0003-2697(79)90690-0).
- [2] Kapuscinski, Jan. 2009. "DAPI: A DNA-Specific Fluorescent Probe." *Biotechnic & Histochemistry*, July. <https://doi.org/10.3109/10520299509108199>.
- [3] Kirillov, Alexander, Eric Mintun, Nikhila Ravi, Hanzi Mao, Chloe Rolland, Laura Gustafson, Tete Xiao, et al. 2023. "Segment Anything." arXiv. <https://doi.org/10.48550/arXiv.2304.02643>.
- [4] Krizhevsky, Alex, Ilya Sutskever, and Geoffrey E. Hinton. 2017. "ImageNet Classification with Deep Convolutional Neural Networks." *Communications of the ACM* 60 (6): 84–90. <https://doi.org/10.1145/3065386>.
- [5] Lecun, Y., L. Bottou, Y. Bengio, and P. Haffner. 1998. "Gradient-Based Learning Applied to Document Recognition." *Proceedings of the IEEE* 86 (11): 2278–2324. <https://doi.org/10.1109/5.726791>.
- [6] Ronneberger, Olaf, Philipp Fischer, and Thomas Brox. 2015. "U-Net: Convolutional Networks for Biomedical Image Segmentation." arXiv. <https://doi.org/10.48550/arXiv.1505.04597>.
- [7] Greenwald, N.F., Miller, G., Moen, E. et al. Whole-cell segmentation of tissue images with human-level performance using large-scale data annotation and deep learning. *Nat Biotechnol* 40, 555–565 (2022). <https://doi.org/10.1038/s41587-021-01094-0>
- [8] Bannon, D., Moen, E., Schwartz, M. et al. DeepCell Kiosk: scaling deep learning-enabled cellular image analysis with Kubernetes. *Nat Methods* 18, 43–45 (2021). <https://doi.org/10.1038/s41592-020-01023-0>
- [9] Bannon, D., Moen, E., Schwartz, M. et al. DeepCell Kiosk: scaling deep learning-enabled cellular image analysis with Kubernetes. *Nat Methods* 18, 43–45 (2021). <https://doi.org/10.1038/s41592-020-01023-0>
- [10] *Accurate cell tracking and lineage construction in live-cell imaging experiments with deep learning* Erick Moen, Enrico Borba, Geneva Miller, Morgan Schwartz, Dylan Bannon, Nora Koe, Isabella Camplisson, Daniel Kyme, Cole Pavelchek, Tyler Price, Takamasa Kudo, Edward Pao, William Graf, David Van Valen bioRxiv 803205; doi:<https://doi.org/10.1101/803205>
- [11] Van Valen DA, Kudo T, Lane KM, Macklin DN, Quach NT, DeFelice MM, et al. (2016) Deep Learning Automates the Quantitative Analysis of Individual Cells in Live-Cell Imaging Experiments. *PLoS Comput Biol* 12(11): e1005177. <https://doi.org/10.1371/journal.pcbi.1005177>

---

<sup>1</sup> <https://github.com/Dystopians/CfosCraft/>



